eprints@whiterose.ac.uk
https://eprints.whiterose.ac.uk/

Planar InAs photodiodes fabricated using He ion implantation

Ian Sandall,[1,*] Chee Hing Tan,[1,3] Andrew Smith,[2] and Russell Gwilliam[2]

[1]Department of Electronic and Electrical Engineering, University of Sheffield, Mappin Street, Sheffield, S1 3JD, UK
[2]Ion Beam Centre, University of Surrey, Guildford, Surrey, GU2 7XH, UK
[3]c.h.tan@sheffield.ac
*i.sandall@sheffield.ac.uk

Abstract: We have performed Helium (He) ion implantation on InAs and performed post implant annealing to investigate the effect on the sheet resistance. Using the transmission line model (TLM) we have shown that the sheet resistance of a p^+ InAs layer, with a nominal doping concentration of $1x10^{18}$ cm^{-3}, can increase by over 5 orders of magnitude upon implantation. We achieved a sheet resistance of $1x10^5$ Ω/Square in an 'as-implanted' sample and with subsequent annealing this can be further increased to $1x10^7$ Ω/Square. By also performing implantation on p-i-n structures we have shown that it is possible to produce planar photodiodes with comparable dark currents and quantum efficiencies to chemically etched reference mesa InAs photodiodes.

References and links

1. I. Baker, S. Duncan, and J. Copley, "A low noise, laser-gated imaging system for long range target. identification," Proc. SPIE **5406**, 133–144 (2004).
2. A. Krier, H. H. Gao, and Y. Mao, "A room temperature photovoltaic detector for the mid -infrared (1.8–3.4 μm) wavelength region," Semicond. Sci. Technol. **13**(8), 950–956 (1998).
3. M. Achour, "Free-space optics wavelength selection: 10 μm versus shorter wavelengths," Proc. SPIE **5160**, 234–246 (2004).
4. A. R. J. Marshall, C. H. Tan, M. J. Steer, and J. P. R. David, "Electron dominated impact ionization and avalanche gain characteristics in InAs photodiodes," Appl. Phys. Lett. **93**(11), 111107 (2008).
5. A. R. J. Marshall, P. Vines, P. J. Ker, J. P. R. David, and C. H. Tan, "Avalanche multiplication and excess noise in InAs electron avalanche photodiodes at 77 K," IEEE J. Quantum Electron. **47**(6), 858–864 (2011).
6. P. J. Ker, A. R. J. Marshall, A. B. Krysa, J. P. R. David, and C. H. Tan, "Temperature dependence of leakage current in InAs avalanche photodiodes," IEEE J. Quantum Electron. **47**(8), 1123–1128 (2011).
7. J. M, Arias, J. G. Pasko, M. Zandian, S. H. Shin, G. M. Williams, L. O. Bubulac, R. E. de Wames, and W. E. Tennant, "MBE HgCdTe heterostructure p-on-n planar infrared photodiodes," J. Electron. Mater. **22**, 1049–1053 (1993).
8. R. Wollrab, A. Bauer, H. Bitterlich, M. Bruder, S. Hanna, H. Lutz, K.-M. Mahlein, T. Schallenberg, and J. Ziegler, "Planar n-on-p HgCdTe FPAs for LWIR and VLWIR applications," J. Electron. Mater. **40**(8), 1618–1623 (2011).
9. A. Säynätjoki, P. Kostamo, J. Sormunen, J. Riikonen, A. Lankinen, H. Lipsanen, H. Andersson, K. Banzuzi, S. Nenonen, H. Sipilä, S. Vaijärvi, and D. Lumb, "InAs pixel matrix detectors fabricated by diffusion of Zn in a metal-organic vapour-phase epitaxy reactor," Nucl. Instrum. Methods Phys. Res. A **563**(1), 24–26 (2006).
10. J. W. Shi, F. M. Kuo, and B. R. Huang, "Zn-diffusion InAs photodiodes on a semi-insulating GaAs substrate for high-speed and low dark-current performance," IEEE Photon. Technol. Lett. **23**(2), 100–102 (2011).
11. A. Ezis and D. W. Langer, "Backgating characteristics of MODFET structures," IEEE Electron Device Lett. **6**(10), 494–496 (1985).
12. J. D. Speight, P. Leigh, N. Mcintyre, I. G. Groves, S. O'Hara, and P. Hemment, "High-efficiency proton-isolated GaAs IMPATT diodes," Electron Lett. **10**(7), 98–99 (1974).
13. J. J. Hsieh, J. A. Rossi, and J. P. Donnelly, "Room-temperature cw operation of GaInAsP/InP double-heterostructure diode lasers emitting at 1.1 μm," Appl. Phys. Lett. **28**(12), 709–711 (1976).
14. M. V. Rao, "High-energy (MeV) ion implantation and its device applications in GaAs and InP," IEEE Trans. Electron. Dev. **40**(6), 1053–1066 (1993).

15. S. Ahmed, B. J. Sealy, and R. Gwilliam, "Annealing characteristics of the implant-isolated n-type GaAs layers: effects of ion species and implant temperature," Nucl. Instrum. Methods Phys. Res. B **206**, 1008–1012 (2003).
16. S. Ahmed, R. Gwilliam, and B. J. Sealy, "Ion-beam-induced isolation of GaAs layers by ^{4}He$^+$ implantation: effects of hot implants," Semicond. Sci. Technol. **16**(10), L64–L67 (2001).
17. A. G. Foyt, W. T. Lindley, and J. P. Donelly, "*n-p* Junction photodetectors in InSb fabricated by proton bombardment," Appl. Phys. Lett. **16**(9), 335–337 (1970).
18. S. J. Pearton, "Ion implantation doping and isolation of III-V semiconductors," Nucl. Instrum. Methods Phys. Res. B **59–60**, 970–977 (1991).
19. P. Too, S. Ahmed, R. Gwilliam, and B. J. Sealy, "Electrical isolation of InP and InGaAs using iron and krypton," Electron. Lett. **40**(20), 1302–1303 (2004).
20. H. Boudinov, H. H. Tan, and C. Jagadish, "Electrical isolation of *n*-type and *p*-type InP layers by proton bombardment," J. Appl. Phys. **89**(10), 5343–5347 (2001).

1. Introduction

The infrared spectral region between 1.5 and 3.5 µm is of great interest for a number of applications including military imaging [1], gas sensing [2] and free space communications [3]. Recently InAs has been demonstrated to operate as an excellent avalanche photodiode (APD) over this spectral range with single carrier multiplication and low excess noise [4, 5]. However current commercial InAs photodiodes, for example the Judson J12 series, cannot be operated in the avalanche mode due to a rapid increase of dark current with bias.

Previously reported InAs mesa APDs have been fabricated using wet chemical etching techniques [4]. While at room temperature the bulk current is dominant in these APDs with diameters above 50 µm, further improvement in the fabrication is desirable to suppress the surface leakage current in small area APDs, such as 25 µm x 25 µm or smaller to pave the way for development for InAs APD arrays [6]. In addition the surface leakage becomes increasingly dominant as the bulk current reduces at low temperature hindering the low temperature performance of InAs APDs. A potential method to reduce the surface leakage current and hence increase the device reliability is to fabricate planar photodiodes, as commonly employed in the fabrication of HgCdTe photodiodes [7, 8].

One way to achieve a planar device is through the use of Zinc diffusion to define localized p doped regions. This technique has been used previously on InAs to form a pixel matrix of p-n junctions to detect alpha particles [9] and high speed photodiodes grown on GaAs [10]. The dark current of ~1 mA at −1 V was reported in Ref [9]. (but the device size was not provided) while relatively high current density of 5 - 67 Acm^{-2} at −0.1 V in was reported in Ref [10], although it was not clear whether the latter was due to the diffusion process or lattice mismatch with GaAs substrate. These suggest further optimization of Zinc diffusion is necessary to reduce the dark current.

An alternative approach to fabricate planar devices is through the use of ion implantation. This technique has previously been used in wider bandgap semiconductors such as GaAs and InP to form planar devices and define device active regions in the fabrication of HEMTs [11], IMPATT diodes [12] and in defining buried heterostructures in laser diodes [13]. A potential advantage to using ion implantation over a diffusion based technique is the greater flexibility in the species to be implanted, as well as potential to achieve greater depths with good uniformity. The device active regions are formed either by the implantation of a dopant such as Si or Be to form n and p type regions respectively or via the implantation of a compensation ion (e.g. He, O or B) to create highly resistive regions [14]. A number of studies have been performed on the use of He implantation in GaAs to create highly resistive regions [15, 16]. In these studies it was shown that high resistive regions are formed through the creation of deep 'mid-band' traps which restrict the flow of charge. The influence of post implant annealing has also been investigated and was found to further increase the resistivity of such layers by reducing the number of shallow levels thus reducing hopping conduction.

For narrower bandgap semiconductors limited work has been performed as a much smaller increase in resistance is expected due to the introduction of hopping conduction across the bandgap [17, 18]. For example Oxygen implantation into InGaAs results in resistances in

the range $10^4 – 10^5$ Ω/Square [16], while Iron and Krypton implantation have both been used to increase the sheet resistance a further order of magnitude to 10^6 Ω/Square [19]. Additionally investigation of proton implantation in InSb has been shown to result in n-type material becoming p-type, due to traps not being created in the middle of the bandgap [17].

To the best of our knowledge in this paper we present the first study of using He ion implantation to increase the resistance in InAs. We evaluate the effect of implantation and subsequent annealing on the sheet resistance of p-type InAs, before investigating the possibility of using this technique to create planar photodiodes. We perform He implantation in the area around circular p-i-n photodiodes to electrically isolate them and investigate their subsequent electrical and optical properties.

2. Experimental details

2.1 Growth and fabrication details

An InAs sample consisting of a 2 µm p^+ doped ($1x10^{18} cm^{-3}$ of Be) layer, grown on an InAs substrate by Metal Organic Vapour Phase Epitaxy, was implanted with He. Multiple implantation energies and doses were used to create a flat damage distribution of approximately 1.7% up to a depth of just over 2 µm. In total four implantations were used to achieve this with the following conditions 1) 36 keV with a dose of $1.3x10^{13}$, 2) 120 keV at $7.4x10^{13}$, 3) 300 keV at $2.04x10^{14}$ and 4) 600 keV at $4.62x10^{14}$ ions/cm^2. All the implants were performed, at the Surrey Ion Beam Centre, at room temperature and with the wafer at an angle of 7° to minimize channeling of the implanted ions. The implanted sample was then cleaved into various pieces which were annealed in a rapid thermal annealer before depositing TLM pads for subsequent resistivity measurements. All samples were annealed for two minutes and were sandwiched between two InAs carrier wafers to minimize any out diffusion.

The p-i-n structure used was also grown by Metal Organic Vapour Phase Epitaxy consisting a 2 µm n doped layer (Si, $1x10^{17} cm^{-3}$), followed by a 6 µm intrinsic layer and then a 2 µm p doped layer (Be, $1x10^{18} cm^{-3}$). A set of reference pin diodes were fabricated using our standard wet etching recipes [4] of a 1:1:1 (phosphoric acid: hydrogen peroxide: de-ionized water) etch, followed by a finishing etch of 1:8:80 (sulphuric acid: hydrogen peroxide: de-ionized water), to define the mesa diodes with radii between for 25 to 200 µm. For the ion implantation samples a layer of 2.5 µm thick SiN was deposited on a set of diodes with circular metal contacts of various sizes prior to ion implantation using similar ion implant conditions described above. Figure 1 shows a schematic of the implanted structure and an image of the fabricated devices.
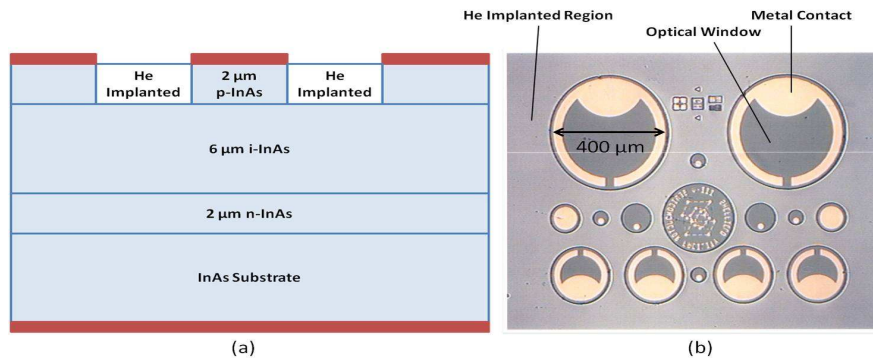

Fig. 1. (a) Schematic of an implanted p-i-n diode, indicating the He implanted regions and (b) representative image of fabricated diodes of various sizes.

2b. Electrical and optical characterization

TLM and current-voltage (IV) measurements were performed using an Agilent B1500 parameter analyzer, after correcting for the resistance of the system. The photocurrent was measured using phase sensitive detection techniques, in which mechanically chopped 1064 nm laser light was focused onto the optical window of the diodes and the resultant photocurrent was measured using a lock-in amplifier. The wavelength of 1064 nm was not critical for conventional photodiode characterization but was selected to ensure the light was fully absorbed in the top p-layer facilitating pure electron injection into the intrinsic region. Pure electron injection is desirable for characterizing the potential of our diode as APD. The incident power was measured using an optical power meter so that the responsivity could be calculated. The ratio of this responsivity to the maximum theoretical responsivity at 1064 nm (0.86 A/W) was calculated to give the external quantum efficiency. For these measurements the excitation spot was focused to a radius of around 20 µm and centred onto devices with radii of either 100 or 200 µm, to ensure that the carrier lifetime in the He implanted region does not influence the measurements. All measurements have been performed at room temperature.

3. Results and discussion

Figure 2 shows the resistivity of the p^+ layer, determined from TLM measurements, as a function of the annealing temperature. It can clearly be seen that upon He implantation the resistivity increases by 5 orders of magnitude compared to the as grown reference p^+ InAs sample. After undergoing annealing a further gradual increase in the resistivity was measured up to a temperature of 450 °C followed by a rapidly reducing value reaching a resistivity value similar to the as grown reference sample at 700 °C.
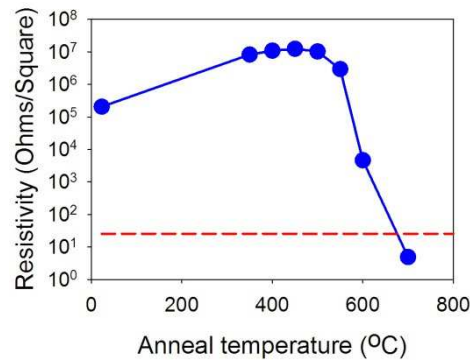

Fig. 2. Resistivity of the He implanted p^+ InAs sample as a function of annealing temperature. The dotted line shows the initial resistivity of an as grown p^+ sample.

This result is similar to the resistance behavior reported for GaAs [15] upon He implantation. This may seem surprising as previous work on narrow bandgaps showed smaller increases [17], due to an increased hopping conduction. However it has previously be shown that the change in resistance can be highly sensitive to the implant species, implant conditions and the polarity of the target material. For example upon ion implantation in InP, sheet resistance values ranging from 10^5 Ω/Square [20] (when using proton implantation at room temperature) to 10^8 Ω/Square (when using Iron implantation at 77 K and utilizing subsequent annealing) [19, 20] have been reported under differing conditions. Therefore investigation of the dependence of resistance in InAs on differing implant conditions is a subject of ongoing work.
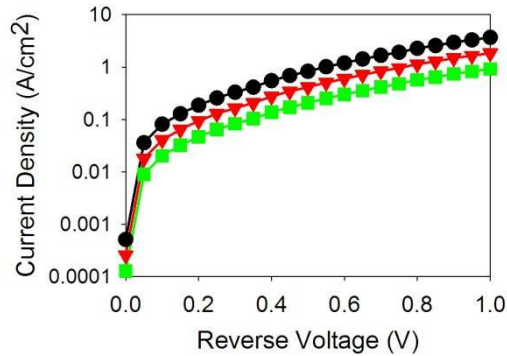
Fig. 3. Dark currents for various 'as-implanted' diodes with radii of 200 (circles), 100 (triangles), 50 (squares).

Our results show that the sheet resistance of p-type InAs can be increased through He implantation. To investigate if this technique can be used to fabricate planar photodiodes we have also performed He implantation on p-i-n diodes. Figure 3 shows the dark current density for a variety of radii for the 'as-implanted' sample, it can clearly be seen that the dark current does not scale with area. We believe that the He implanted regions do not have sufficiently high resistance to isolate neighboring diodes, leading to the poor current density agreement between different sized diodes observed in Fig. 3.
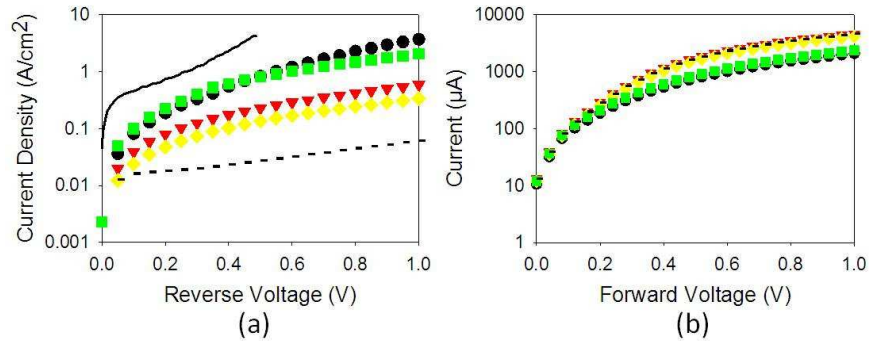

Fig. 4. (a) Measured dark currents and (b) Forward current characteristics for 'as-implanted' (circles), annealed at 350 °C (triangles), 450 °C (diamonds) and 550 °C (squares) diodes with radii of 200 µm. The dashed line shows the dark current from a reference mesa diode fabricated using wet etching, while the solid line shows the dark current from a commercial Judson InAs photodiode (model number: J12-18C-R250U).

From Fig. 2, it was concluded that post implant annealing could increase the resistivity of p-type InAs. Therefore to improve the voltage confinement within the active region we have annealed these He implanted pin diodes at various temperatures over a range between 350 to 550 °C. The measured dark current densities are plotted in Fig. 4(a). The initial 'as-implanted' diode shows an increase in the dark current of around two orders of magnitude at a reverse voltage of 1 V compared to a reference mesa diode (dashed line). This increase in current is likely to be due to the increase in leakage current as the diodes are not fully isolated as discussed previously. This is further supported by the decrease in current observed at annealing temperatures of 350 and 450 °C, corresponding to increased layer resistivity. At the highest annealing temperature of 550 °C the current rises again due to reduced resistivity of the p$^+$ layer. It is interesting to note that dark current densities in all the samples are lower than that of a commercial diode Judson InAs photodiode (model number: J12-18C-R250U).

The forward current characteristics are shown in Fig. 4(b). A large series resistance can be observed to limit the current above a voltage of around 0.25 V. Using standard diode equation in the forward bias we estimated the values of series resistance to be ranging from 400 to 600 Ω. We believe that the origin for such a high resistance is due to the low silicon doping concentration in the bottom n-layer as it is present in the reference etched sample as well as the implanted ones.
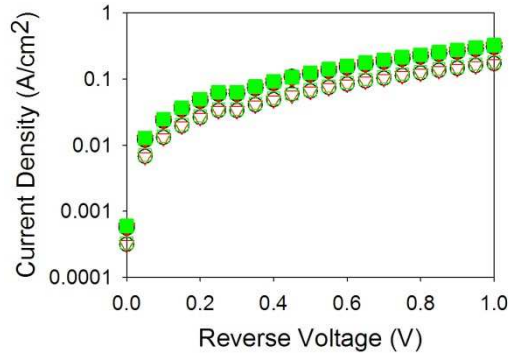

Fig. 5. Dark currents for samples annealed at 350 °C (closed symbols) and 450 °C (open symbols) with different radii diodes sizes (200 (circles), 100 (triangles), 50 (squares)).

Figure 5 shows dark currents for different sized diodes annealed at 350 and 450 °C. The currents for these diodes scale with the area. This indicates that the resistance in the He implanted regions is sufficiently high to electrically isolate the diodes and prevent the voltage from spreading to adjacent diodes. Despite this good agreement between diodes of differing sizes indicating that the dark current is dominated by bulk current contributions, the dark current for the implanted and annealed samples is higher than the reference etched diode shown in Fig. 4(a). We believe that this increase in the bulk current may be due to He ions penetrating into the active region. Although the circular diode was masked with 2.5 µm of SiN, it is possible that some of the higher energy He ions have entered the diode active region as the He ions are extremely light.
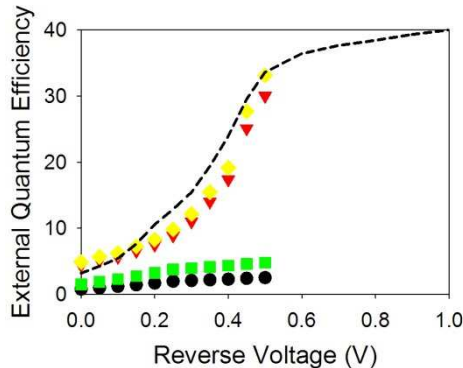

Fig. 6. External Quantum efficiency as a function of voltage at an excitation wavelength of 1064 nm for the as implanted device (circles) and devices annealed at 350 °C (triangles), 450 °C (diamonds) and 550 °C (squares). The dashed line shows the efficiency from a reference mesa diode.

To further investigate the device potential we have also measured the external quantum efficiency at low voltages, as shown in Fig. 6. All the diodes show an increase in the efficiency as the voltage is increased from 0 to 0.5 V. The values obtained in the reference

mesa diode as well as those implanted and annealed at 350 and 450 °C are similar. This increasing efficiency is attributed to the increase in carrier collection efficiency as the depletion region widens with bias voltage. The efficiency approaches 40% at high bias voltage. The 'as-implanted' and the 550 °C annealed samples show a dramatic decrease in the efficiency. The fall in efficiency in these diodes seems surprising, as the He was implanted into regions surrounding the devices and was not expected to influence the optical performance.

We believe this low quantum efficiency may be qualitatively explained by the large RC time constant in the 'as-implanted' and 550 °C samples due to poor electrical confinement. Figure 7 illustrates the equivalent electrical circuit of 3 neighboring diodes. Each diode is represented by a current source, I_d, in parallel with a resistor, R_d, and a capacitor, C_d, as well as a series resistor, R_s. A neighboring diode is connected by a resistor R_i which depends on the resistivity of the implanted region and the distance between the two neighboring diodes. For the standard etched reference diode R_i can be assumed to be infinitely large as the surrounding material has been removed. Therefore the RC time constant of a particular diode is controlled by C_d, R_s and the value of the load resistor. In the reference mesa diodes the RC values are sufficiently small leading to a sufficiently larger diode bandwidth compare to the modulation frequency of 185 Hz. Measurement of the diode bandwidth will require a different mask set with appropriate bond pads for microwave probing.
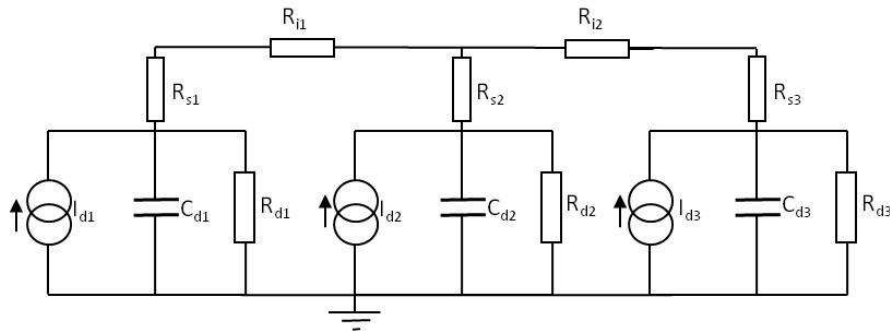

Fig. 7. Equivalent electrical circuit for 3 diodes.

For the implanted samples R_i will be governed by the sheet resistance. From Fig. 2 the 'as-implanted' and 550 °C samples have low resistivities and therefore a low R_i is expected. Consequently all the diodes, on our 1 cm x 1 cm dies, are linked, producing a much larger effective capacitance than an individual diode. Our forward current-voltage characteristics in Fig. 4(b) suggest that the series resistance R_s is ~400-600 Ω which is relatively large due to the relatively low Si doping in the bottom n layer. If R_i is assumed to be zero, the effective RC time constant of a 1 cm x 1 cm die is a few hundred micro seconds leading to a bandwidth of a few hundred Hz, very close to the laser modulating frequency of 185 Hz. As a result, low responsivity was measured in samples with low implanted region resistivities.
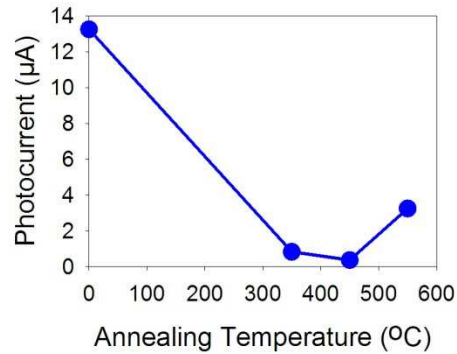
Fig. 8. Photocurrent measured at 0.5 V when light is focused onto an adjacent mesa.

The electrical isolation between adjacent diodes can also be investigated by measuring the photocurrent from a diode while the excitation spot is positioned over an adjacent diode. Figure 8 shows the photocurrent measured in a 200 µm radius diode when the light was focused on a similar sized adjacent diode, (the centre to centre separation is 600 μm) as a function of the annealing temperature. In the 'as-implanted' sample a high photocurrent of 13 µA was measured when the neighboring diode was excited. However as the annealing temperature was increased this current rapidly falls, reaching a minimum of 0.3 µA at an annealing temperature of 450 °C. This result shows that there is a high degree of electrical connection between the diodes for the 'as-implanted' sample. Upon subsequent annealing the electrical isolation improves dramatically reducing the photocurrent. However at the highest annealing temperature the current rises again due to the reduced electrical isolation as the resistance of the He implanted regions reduces.
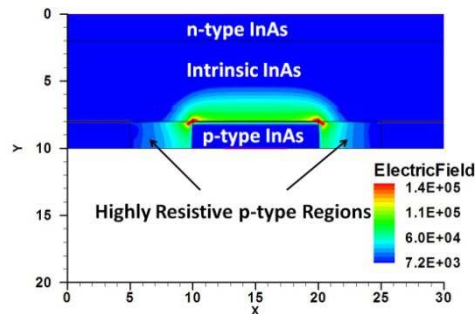

Fig. 9. Simulated electric field for InAs mesa with He implanted regions and annealed at a temperature of 450 °C for a reverse bias of 1 V.

The encouraging results in Fig. 6 have motivated us to evaluate these He implanted diodes in the avalanche mode. Unfortunately we could only apply a reverse bias of 1 V before the diodes showed catastrophic breakdown. We attribute this breakdown to local electric field hot spots due to a non-optimized implantation depth. The peak He implantation depth is only around 2 µm (coinciding with the p-i junction). Consequently a high electric field may form at the junction between the p-doped, intrinsic and implanted regions, which may result in premature edge breakdown. To investigate this further we have modeled the electric field in the device using the commercial software suite DESSIS. The material resistance cannot be modified within DESSIS so to model the implanted regions we have lowered the carrier mobilities by the same order of magnitude as the resistance was seen to increase in Fig. 2. The

simulated field for a sample implanted and annealed at 450 °C at a reverse bias of 1 V is shown in Fig. 9. High electric fields can be observed across the p-i junction, these fields reach peak values at the corners of the implanted regions. The peak electric field is ~150 kV/cm, which is well in excess of the value for the onset of tunneling currents and impact ionization in InAs [5] leading to a sudden and sharp increase in the current and potentially causing the failure of the device when stressed under this high current. These results indicate that for the development of planar InAs APDs either the implantation depth will have to be much deeper or inclusion of guard ring will be required to suppress edge breakdown.

In addition to the optical and electrical characterization we have attempted to assess the diode reliability by performing repetitive reverse IV measurements up to 1 V. We observed a random and sudden breakdown in some of these devices after repeated operation; this takes the form of an abrupt switch in the IV characteristics from diode like behavior to a short circuit. At present the operation lifetime before this breakdown occurs appears to be random. Currently we cannot ascertain the origin of this failure mode since this behavior has not been observed in the reference etched device nor has any change been observed in the resistivity of the implanted layers used for the TLM analysis.

4. Conclusions

This work has shown that it is possible to use He implantation with InAs to produce highly resistive areas and that when combined with post implantation annealing, a sufficiently high resistive region can be formed to allow the fabrication of a planar photodiode. Due to the implantation conditions used in this work an isolation depth of only around 2 µm has been achieved despite the total device thickness being 8 µm. As such this appears to have limited the upper voltage limit that the diodes can be operated to due to the onset of edge breakdown.

We have measured similar external quantum efficiencies for an implanted and subsequently annealed device as we would obtain for a reference etched device. These results also suggest that it may be possible to use implantation techniques to fabricate photodiodes in narrower bandgap materials such as InSb to allow the realization of long wavelength planar detectors.

In summary we have performed He ion implantation into InAs and performed post implant annealing. From TLM measurements we have shown that the sheet resistance of InAs can be dramatically increased. By also performing implantation on p-i-n structures we have shown that it is possible to produce planar photodiodes with comparable efficiencies to reference etched diodes.

Acknowledgments